Diffusion-weighted magnetic resonance imaging detection of basal forebrain cholinergic degeneration in a mouse model of Alzheimer's disease

[1]Georg M Kerbler, [1]Adam S Hamlin, [2,3]Kerstin Pannek, [3]Marianne Keller, [3]Nyoman D Kurniawan, [2,3]Stephen C Rose, [1]Elizabeth J Coulson*

[1]Queensland Brain Institute,

[2]Centre for Clinical Research,

[3]Centre for Advanced Imaging,

The University of Queensland, Brisbane, 4072 Qld. Australia

* Corresponding author:
Associate Professor Elizabeth Coulson
Queensland Brain Institute,
The University of Queensland,
Brisbane, 4072 Qld. Australia
p:+61 71 33466392,
f: +61 7 33466301
e: e.coulson@uq.edu.au

Abbreviations

ChAT: Choline acetyl transferase
dMRI: diffusion MRI
FA: fractional anisotropy
MCI: mild cognitive impairment
MRI: magnetic resonance imaging
$p75^{NTR}$: p75 neurotrophin receptor
PB: phosphate buffer
PBS: phosphate buffered saline
ROI: region of interest
SAP: saporin

Abstract

Loss of basal forebrain cholinergic neurons is an early and key feature of Alzheimer's disease. The aim of this study was to determine whether loss of basal forebrain cholinergic neurons underpins changes detected using diffusion magnetic resonance imaging (dMRI) and probabilistic tractography in a mouse model. The toxin saporin conjugated to a p75 neurotrophin receptor antibody (mu-p75-SAP) was used to induce a specific lesion of the basal forebrain cholinergic neurons (~30% loss) and significant loss of terminal cholinergic projections in the hippocampus in C57Bl/6J mice, as determined by histology. Analysis by dMRI of the basal forebrain revealed a significant increase in anisotropic diffusion parameters in lesioned mice compared with control (Rb-IgG-SAP) animals. These parameters strongly inversely correlated with the number of choline acetyl transferase-positive neurons. Moreover, probabilistic tractography analysis of the septo-hippocampal tracts revealed a trend to significant change in diffusion parameters in lesioned mice. This study illustrates that moderate loss of basal forebrain cholinergic neurons (representing only a minor proportion of all septo-hippocampal axons in our case) can be detected by measuring diffusion parameters of either the basal forebrain nuclei or possibly the basal forebrain tracts, thereby further validating the feasibility of dMRI and probabilistic tractography as non-invasive tools for diagnosing Alzheimer's disease in humans.

Keywords

Cholinergic basal forebrain, tractography, p75 neurotrophin receptor, MRI, diffusion weighted imaging, neurodegeneration

1. Introduction

The basal forebrain is a key modulator of neurotransmission, function and plasticity of the hippocampus and amygdala, as well as the entire cortical mantle (Mesulam et al., 1983), and is strongly implicated in regulating attention, learning and memory (Mufson, 2003). Loss of the cholinergic neurons of the basal forebrain is a pathological hallmark of Alzheimer's disease at autopsy (Mufson et al., 2002; Whitehouse et al., 1982). Furthermore, numerous studies have shown that degeneration of the basal forebrain is linked, albeit indirectly, to early signs of cognitive decline in Alzheimer's disease patients, including deficits in spatial navigation and memory (George et al., 2009; Grothe et al., 2011; Grothe et al., 2010; Muth et al., 2010). In these studies, magnetic resonance imaging (MRI) methods were used to detect structural changes associated with atrophy of the basal forebrain, particularly in the posterior regions (Grothe et al., 2011), these changes being correlated with cognitive decline in clinical cohorts of patients diagnosed with Alzheimer's disease or its prodromal stage, mild cognitive impairment (MCI). In some cases, basal forebrain atrophy was observed as early as 4.5 years before the onset of overt clinical symptoms (Hall et al., 2008).

By the time atrophy of a structure can be detected as a volumetric reduction with structural MRI, significant cell and tissue loss has already occurred. The drugs currently prescribed for the treatment of Alzheimer's disease, inhibitors of acetyl cholinesterase, enhance basal forebrain cholinergic function by inhibiting the degradation of acetylcholine produced by the surviving neurons. However, as the diagnosis of MCI or Alzheimer's disease currently occurs at a stage at which the cholinergic system has been irreversibly damaged, it is not surprising that these drugs have mild to little effect in prolonging cognitive function (Mancuso et al., 2011). Non-invasive early detection of basal forebrain neurodegeneration prior to overt tissue loss therefore has the potential to improve the window of efficacy of acetylcholine esterase inhibitors for the treatment of Alzheimer's disease.

Diffusion MRI (dMRI) is a technique that can be used to analyze differences in structural integrity and brain connectivity, and has been successfully employed to

detect differences between Alzheimer's patients and healthy control subjects (Kiuchi et al., 2009; Pievani et al., 2010; Teipel et al., 2010). dMRI measures water diffusion within a tissue, with common dMRI measures including fractional anisotropy (FA), a measure of the degree of diffusion anisotropy where a value of zero means that diffusion is unrestricted (or equally restricted) and a value of one means that diffusion only occurs along one axis and is fully restricted in all other directions, mean diffusivity, a measure describing the extent of free diffusion without assuming a particular direction, axial diffusivity (AD; also known as parallel diffusivity), a measure of the extent of water moving along the primary axis of diffusion, and radial diffusivity (RD; also known as perpendicular diffusivity), a measure of water movement along the minor axes perpendicular to the primary axis. These dMRI parameters can be extracted for individual brain regions as well as for streamlines generated from dMRI data by tractography, a technique that is used to infer the connectivity of the brain, particularly of white-matter tracts (Mori and Zhang, 2006).

Based on the idea that cholinergic axons become dystrophic prior to neuronal degeneration (Ypsilanti et al., 2008), the aim of the current study was to determine whether mild to moderate loss of basal forebrain cholinergic nuclei and axons could underpin changes to dMRI measures and tractography prior to the point at which changes correlate with overt atrophy. In order to investigate this, we used a mouse model in which the toxin saporin, conjugated to an antibody to a receptor almost exclusively expressed by basal forebrain cholinergic neurons (p75 neurotrophin receptor; $p75^{NTR}$), is injected into the ventricles (Berger-Sweeney et al., 2001). This treatment has been demonstrated to provide a robust model of the selective basal forebrain cholinergic neuron loss and behavioral consequences seen in Alzheimer's disease (Berger-Sweeney et al., 2001; Kokjohn and Roher, 2009; Moreau et al., 2008; Nilsson et al., 1992; Perry et al., 2001; Rossner, 1997). We hypothesized that all dMRI measures of the basal forebrain nuclei, together with the diffusion measures but not track number *per se* of septo-hippocampal tractograms, would be altered to reflect the neurodegeneration induced by this model.

2. Materials and Methods

2.1 Animals

Experimentally naive male C57Bl/6J mice were housed in groups of four and maintained on a 12 h light/dark cycle, with food and water *ad libitum*. All procedures were approved by the University of Queensland Animal Ethics Committee.

2.2 Surgery

Eight 8-10 week old male C57Bl/6J mice (22-24g) were anesthetized by intraperitoneal (i.p.) injection with a mixture of ketamine (130 mg/kg) and the muscle relaxant xylazine (6 mg/kg). Each mouse was then placed in a stereotaxic frame (with the incisor bar maintained at -3.3 mm below horizontal to achieve a flat skull position). Bilateral infusions of mu-p75-saporin or control rabbit-IgG-saporin dissolved in phosphate buffered saline (PBS; 0.2 µg/ventricle; Advanced Targeting Systems, San Diego, CA) were performed using a 30G needle attached to a 5µl Hamilton syringe. The needle was lowered into the lateral ventricle using the following co-ordinates: A-P, -0.3 mm; M-L, ±1.0 mm; D-V, −2.0 mm from Bregma; (Franklin and Paxinos, 2007). Infusions were conducted over 5 min, after which the needle was left in place for 10 min to allow for diffusion. Immediately after surgery, mice were injected subcutaneously (s.c.) with the analgesic torbogesic (1.3 mg/kg), and the antibiotic Baytril® (0.43 mg/kg).

Fourteen days post-surgery mice were deeply anesthetized with sodium pentobarbital (100 mg/kg i.p.) and perfused transcardially with 20 ml of 0.9% saline, containing 1% sodium nitrite and heparin (5000 I.U./ml), followed by 100 ml of 4% paraformaldehyde in 0.1 M phosphate buffer (PB), pH 7.4. Brains were post-fixed overnight in the same fixative, followed by repeated washing in PBS (pH 7.4) for 4 days prior to MRI acquisition.

2.3 MRI acquisition

After perfusion, mouse brains were washed in PBS for 4 days, after which they were immersed in Fomblin oil (Y06/6 grade, Solvay, NY) and diffusion weighted

magnetic resonance images were acquired according to the protocol of Moldrich et al. (2010). Briefly, we used a small animal MRI system (16.4 T vertical bore; Bruker Biospin, Rheinstetten, Germany; ParaVision v5.0) with a 15 mm linear SAW coil (M2MImaging, Brisbane, Australia). 3D DWspin-echo sequences were acquired with TR/TE = 400ms/22.3 ms, NEX=1 and a signal average of 1. We acquired thirty high diffusion-weighted images (b=5000 s/mm^2) as well as two low diffusion weighted (b=0 s/mm^2) images for each mouse brain with encoding gradient (δ/Δ=25/14 ms) vectors uniformly distributed using the electrostatic approach (Jones et al., 1999). Resolution was set at 100 µm isotropic (uninterpolated) and total imaging time was 16 h.

2.4 Basal forebrain mask

Reconstruction was performed using MRtrix (v0.2.9, www.nitrc.org/projects/mrtrix). Regions of interest (ROIs) were drawn manually on 12 consecutive coronal slices using color-coded FA maps generated by diffusion tensor imaging (DTI) reconstruction of the diffusion data. Using the mouse brain atlas of Franklin and Paxinos (2007) as guidance, ROIs of the basal forebrain were drawn, starting with the second slice anterior to the first slice where the genu of the corpus callosum is connected through the midline (approximately 1.34 mm anterior to Bregma) and finishing before the anterior commissure crosses the midline (approximately 0.26 mm anterior to Bregma), thereby assuring that the mask predominately encompassed the medial septum and the vertical and horizontal diagonal bands of Broca. The anterior-posterior distance covered was 1200 µm (12 slices of 100 µm). The average size of the ROI did not differ significantly between the control and lesioned groups (see section 3.2). The basal forebrain mask was used to extract FA, mean diffusivity, axial diffusivity and radial diffusivity.

2.5 Tractography

MRtrix (v0.2.9, www.nitrc.org/projects/mrtrix) was used to perform constrained spherical deconvolution (CSD) and to generate the fiber orientation distribution (FOD). Probabilistic tractography was performed with MRtrix, creating whole

brain tractograms by seeding every voxel five times and using tracking parameters optimized for mouse brain (step size = 0.01 mm, curvature = 0.07 mm, seeds/voxel = 5; (Moldrich et al., 2010).

Basal forebrain streamlines were then extracted by applying the basal forebrain mask to the whole brain tractograms. To image streamlines that project from the basal forebrain through the fimbria/fornix to the hippocampus, but not including cortical areas, a hippocampal waypoint ROI was created at approximately -2.60 mm posterior to Bregma. This hippocampal waypoint ROI, together with additional exclusions used in conjunction with the basal forebrain mask, eliminated false positive streamlines such as the stria terminalis and the optic tract.

To test whether the streamline changes were selective for the basal forebrain tracts, we performed tractography on a control tract, the inferior cerebellar peduncle. Bilateral ROIs were drawn on color-coded FA maps on three consecutive slices from approximately -6.00 to -6.24 mm posterior to Bregma, using the mouse brain atlas of Franklin and Paxinos (2007) as guidance. Inferior cerebellar peduncle streamlines were obtained by applying the ROI to whole brain tractograms.

The measure streamline number was normalized to the voxel number of the corresponding ROI. A threshold of 15 streamlines (determined empirically) was used to measure track volume. In addition, FA, mean diffusivity, axial diffusivity and radial diffusivity were extracted from the tracks using the individual tracks for sampling.

2.6 Volumetric measurements

The hippocampal volume was measured using itk-snap (www.itksnap.org) and normalized to the brain volume (excluding olfactory bulbs, cerebellum and brainstem, to avoid areas that possibly got damaged during brain removal).

2.7 MRI data analysis

An unpaired two-tailed non-parametric t-test (Mann-Whitney, CI = 95%) was

used to determine significant differences of means for basal forebrain mask and tractography diffusion measures. For correlations, a non-parametric correlation of regression (Spearman) analysis was used. False discovery rate ($\alpha = 0.1$) was used to correct for multiple comparisons.

2.8 Immunohistochemistry

Immediately following scanning (see section 2.2) brains were placed in 20% sucrose solution overnight. Brains were blocked using a matrix (Stoelting Co., Wood Dale, IL), aligned to the atlas of Franklin and Paxinos (2007), and 40 µm coronal sections were cut in three serially adjacent sets through the basal forebrain and hippocampus using a sliding microtome (SM2000r, Leica, Sydney, Australia). Sections were stored in 0.1% sodium azide in 0.1 M PBS.

One series of sections was used to reveal choline acetyltransferase (ChAT) using peroxidase immunohistochemistry. Free-floating sections were washed repeatedly in 0.1 M PB, followed by two 30 min washes in 50% ethanol, the second of which contained 3% H_2O_2. Sections were then incubated in 5% normal horse serum (NHS) in PB for 30 min, followed by incubation with goat anti-ChAT antibody (1:3000; Millipore, Billerica, MA), diluted in 0.1 M PB containing 0.1% sodium azide, 2% NHS and 0.2% Triton X-100 (PBT-X), for 48 h at 4 °C with gentle agitation. After washing, sections were incubated overnight at room temperature in biotinylated donkey anti-goat IgG (1:1000; Jackson Immunoresearch Laboratories, West Grove, PA) diluted in 2% NHS PBT-X. Sections were then incubated for 2h at room temperature in ABC reagent (Vector Elite kit: 6 µl/ml avidin and 6 µl/ml biotin; Vector Laboratories, Burlingame, CA). Black immunoreactive cytoplasm labeled for ChAT was revealed by a nickel-intensified diaminobenzidine reaction, with peroxide being generated by glucose oxidase. First, sections were washed in PB, followed by 0.1 M acetate buffer, and then incubated for 15 min in 0.1 M acetate buffer (pH 6.0) containing 2% nickel sulfate, 0.0025% 3,3-diaminobenzidine, 0.004% ammonium chloride, and 0.02% d-glucose. The peroxidase reaction was started by adding glucose oxidase (0.2 µl/ml) and stopped using acetate buffer (pH 6.0). Brain sections were then

washed in PB. Sections were mounted onto chrome-alum/gelatin-treated slides, dehydrated, cleared in histolene, and coverslipped with DePeX.

A series of sections through the basal forebrain of lesioned and control mice was used to immunohistochemically label parvalbumin. Free-floating sections were washed repeatedly in PBS, followed by a 2h incubation in PBS containing 10% NHS and 0.5% Triton X-100. Mouse anti-parvalbumin (1:1000; Millipore, Temecula, CA), diluted in 0.1 M PBS containing 0.1% sodium azide, 2% NHS and 0.2% Triton X-100, was then added to the sections, which were incubated for 48 h at room temperature, with gentle agitation. After washing, sections were incubated for 4 h at room temperature in donkey anti-mouse FITC (1:200; Jackson Immunoresearch Laboratories), diluted in 2% NHS PBT-X. After washing, sections were mounted onto chrome alum/gelatin-treated slides and coverslipped with buffered glycerol (pH 8.6).

2.9 Neuronal counting

Bilateral counts of neurons immunoreactive for ChAT were conducted through the rostro-caudal extent of the basal forebrain beginning 1.42 mm from Bregma (Franklin and Paxinos, 2007). Sections were 120 µm apart, with five sections being counted for the medial septum, four for the vertical diagonal band of Broca (beginning at section 3 of the medial septum) and five for the horizontal diagonal band of Broca (beginning at the end of the vertical diagonal band of Broca) by a researcher blind to the experimental conditions.

Counts of parvalbumin-positive ($p75^{NTR}$-negative) neurons were analyzed as above using images of sections of mu-p75-saporin and Rb-IgG-saporin injected brains. Eight-bit monochrome images were taken of the basal forebrain sections beginning 1.42 mm from Bregma. Images were captured using a Zeiss Axio Imager Z1 and AxioVision v4.8 software, before being exported into ImageJ software (NIH) where bilateral counts of parvalbumin-positive nuclei were conducted by a researcher blind to the conditions.

Differences in the mean number of ChAT-immunoreactive and parvalbumin-immunoreactive cells counted for each region of the basal forebrain per animal

per group were analyzed using ANOVA.

3. Results

3.1 Mu-p75-SAP induced specific lesion of the cholinergic basal forebrain

To selectively ablate basal forebrain cholinergic neurons, mice were injected with saporin conjugated to either a $p75^{NTR}$ antibody (mu-p75-SAP), or to a rabbit IgG (Rb-IgG-SAP) as a control. Following MRI scans, the extent and specificity of the lesion was determined by immunohistological analysis of the medial septum and the vertical and horizontal diagonal bands of Broca (Figure 1). These regions contain approximately equal numbers of cholinergic neurons, which express $p75^{NTR}$ (Mufson et al., 1989), and non $p75^{NTR}$ -expressing GABAergic neurons (Wainer et al., 1985). Both neuronal populations provide input to the hippocampus through the fimbria/fornix.

While no overt atrophy of the structure was appreciable, a significant loss of approximately 30% of ChAT-positive (cholinergic) cells in the medial septum, and the vertical and horizontal diagonal bands of Broca was observed in the lesioned animals (Figure 1A, 1C). We also observed a clear reduction in ChAT-positive terminal labeling in the hippocampus of the lesioned mice (Figure 1C), indicating that the septo-hippocampal cholinergic system was functionally impaired in these animals.

To determine if the treatment caused a specific loss of the cholinergic cells in the basal forebrain we also quantified the number of GABAergic neurons, visualized by parvalbumin staining, in the medial septum, and the vertical and horizontal diagonal bands of Broca (Figure 1B; 1D). This analysis revealed no significant effect of mu-p75-SAP injections compared to Rb-IgG-SAP treatment on parvalbumin-positive neuron number (Figure 1B, 1D), indicating that we had achieved a specific lesion of basal forebrain cholinergic neurons.

3.2 Increased diffusion in the basal forebrain inversely correlated to cholinergic neurodegeneration

To determine whether the lesion could be detected by MRI measures, the basal forebrain diffusion MRI parameters for each of the brains were analyzed. Firstly,

individual basal forebrain masks were created (Figure 2A; 2B, see section 2.3). These encompassed the medial septum and the vertical and horizontal diagonal bands of Broca (Figure 2C, D). The color-coded FA map in combination with the mouse brain atlas was used to create masks of the basal forebrain for each brain according to nearby landmarks. Given the lack of specific anatomical boundaries observable by MRI contrast, the masks by definition also contained minor parts of the lateral diagonal band of Broca (also called the magnocellular preoptic nucleus), as well as the basal part of the substantia innominata in the posterior section of the mask (ventral part of the mask in Figure 2E).

Given the time between induction of the lesion and imaging, we did not expect or observe by histology overt atrophy of the basal forebrain. This was confirmed when we compared the size of the masks between groups, which revealed no significant difference in voxel number for control animal masks compared with the masks of lesioned animals (control: 882 ± 21 voxels; lesion: 902 ± 27 voxels; n = 4, mean ± SEM). Furthermore given the extent of the lesion, we did not expect atrophy of the hippocampus to occur, caused by the degeneration of cholinergic neurons. Comparison of normalized hippocampal volume between lesioned and control groups revealed no statistically significant difference (control: 25.00 ± 0.56; lesion: 25.04 ± 0.63, n = 4, mean ± SEM).

We hypothesized that the altered tissue characteristics induced by the neuronal loss in lesioned animals would result in increased diffusivity in the affected area. Mean FA, mean diffusivity, axial diffusivity and radial diffusivity within the basal forebrain mask area were extracted for each mouse and group averages were calculated and compared for significant differences. This analysis revealed that all diffusion metrics were significantly increased for the basal forebrain area in the lesioned group compared to the control group. Specifically, the mean values for FA (Figure 3A), mean diffusivity (Figure 3B), axial diffusivity (Figure 3C) and radial diffusivity (Figure 3D) were all significantly higher in the lesioned animals.

To determine the correlation between histological measures and dMRI-associated changes in response to basal forebrain cholinergic neuron loss, we

performed nonparametric correlation of regression analysis of the ChAT-positive neuron numbers and diffusion parameters (Figure 3 E-H). This revealed that all diffusion measures were significantly inversely correlated to ChAT-positive neuron number (Figure 3 E-H), in particular the increase in FA (Figure 3E). This indicates that dMRI parameters such as FA, mean diffusivity, axial diffusivity and radial diffusivity are sensitive measures of neuronal lesions and reflect the degree of neurodegeneration.

3.3 Tractography streamlines showed possible decreased integrity

We next investigated whether a significant reduction in septo-hippocampal connectivity could be detected in the lesioned group of animals. In order to analyze the streamlines connecting the basal forebrain and hippocampus, whole brain tractograms of mice were created using MRtrix. The basal forebrain mask and a hippocampal mask (Figure 4A; see section 2.3) were then applied to the tractograms to delineate the streamlines between these two structures via the fimbria/fornix. The resulting streamlines (Figure 4 A-C) were anatomically verified (Figure 4D) as innervating the alveus and the oriens layer of the hippocampus and, to a lesser degree, other regions of the hippocampus such as the CA3 region and the dentate gyrus (Cole and Nicoll, 1984).

Having established a septo-hippocampal connection, we analyzed the septo-hippocampal streamlines (Figure 5) in each mouse by comparing FA, mean diffusivity, axial diffusivity, and radial diffusivity, as well as track volume, streamline length and streamline number between the control and lesioned groups. This revealed an increase in radial diffusivity ($p = 0.03$, Figure 5C) and trend toward an increase in mean diffusivity ($p = 0.06$, Figure 5D) in the lesioned group, but neither measure was significantly different from the average of the control group following correction for multiple comparisons. No significant differences were observed in FA (Figure 5A) and axial diffusivity (Figure 5B), or in track volume, streamline length or normalized streamline number (Table 1).

Finally, to control for the diffusion changes being selective for the basal forebrain tracts, we performed tractography analysis on a cerebellar tract (see section 2.4),

namely the inferior cerebellar peduncle (Figure 6A,B), which we reasoned should not be affected by either the application of mu-p75-SAP or the surgery. Our comparison revealed no differences in measures of streamline FA, axial diffusivity, radial diffusivity, or mean diffusivity (Figure 6C-F), nor in track volume, streamline length and streamline number (Table 2) of the inferior cerebellar peduncle. This indicated that the p75-directed toxin did not induce systemic axonal degeneration in the mouse brain but caused a specific lesion of basal forebrain cholinergic neurons, which could be detected by tractography of the septo-hippocampal streamlines.

4. Discussion

In this study we used a robust animal model of specific cholinergic lesion of the septo-hippocampal system, mimicking the loss and denervation of basal forebrain cholinergic neurons observed in Alzheimer's disease (Rossner, 1997). We produced a ~30% reduction in this cholinergic pathway, which mimics mild pathology, and therefore possibly MCI or the prodromal stage of Alzheimer's disease rather than severe late-stage loss of basal forebrain cholinergic neurons (Mufson et al., 2002). Despite the small number of experimental animals (n = 4 per group) dMRI was able to detect this mild basal forebrain neurodegeneration. This minor change in total neuron number in the basal forebrain nuclei, was clearly identified on the high-resolution dMRI scans. A total of four diffusion parameters, FA, mean diffusivity, axial diffusivity and radial diffusivity, showed a significant increase within the basal forebrain area and all of these measures significantly inversely correlated to the basal forebrain cholinergic neuron count. As the FA parameter showed the greatest effect, we propose that this provides an extremely accurate and sensitive measure to determine the extent of tissue lesion prior to detection of volumetric changes.

In general, increases in mean, axial and radial diffusivity are well-established features of neuronal degeneration (Filippi and Agosta, 2011). However it has been shown that neuronal degeneration usually results in a decrease of water anisotropy or FA in the affected regions (i.e. a less preferred direction of diffusion; Filippi and Agosta, 2011). In contrast we observed an increase in FA in the lesioned group compared to control. This can be explained by the direct relationship of the FA to the axonal/microscopic organization within a voxel. FA in the basal forebrain tissue reflects cell bodies and axons, innervating axons of posterior brain regions such as the pons, as well as axons from the locus coeruleus which also pass through the basal forebrain en route to the cortex (Sara, 2009). In this tissue, a proportion of the axons, including cholinergic axons, are crossing over other axons. Therefore the FA consists of multiple incoherent diffusion orientations. Once a significant number of basal forebrain cholinergic neurons and their axons have degenerated, due to lesioning, one diffusion

direction maybe selectively removed, and the tissue may therefore appear to have relatively higher directional diffusion along the remaining neuronal tracks, resulting in a higher FA in the lesioned group compared to the control. This phenomenon of increased FA in pathological conditions has been previously documented (Jones, 2010; Tuch et al., 2005) and highlights the fact that interpretation of diffusion parameters must be carried out with reference to the nature of the pathology and the composition of the tissue being examined.

The present study also demonstrates that diffusion MR tractography has the potential to be an extremely sensitive measure of cholinergic degeneration. Probabilistic tractography measures of projections between the basal forebrain nuclei and the hippocampus via the fimbria/fornix showed promise in detecting changes in streamline characteristics induced by loss of cholinergic axons, revealing trends toward significant increases in streamline mean diffusivity and streamline radial diffusivity. A significant number of axonal tracts project through the fornix, of which the cholinergic axons that were affected by the lesion make up only a minor proportion, possibly 15%. Because of this, we were not surprised to observe no changes in measures such as FA, number of streamlines, track volume or streamline length.

Of the factors that can influence diffusion anisotropy, intra-axonal organization appears to have the greatest influence (Pierpaoli et al., 1996). However, other features, such as the density of fiber and glial cell packing, degree of myelination, and individual fiber diameter, may also play a role (Melhem et al., 2002). We observed trends toward a significant increase in radial diffusivity and mean diffusivity, of which the change in radial diffusivity was significant before correcting for multiple comparisons. This suggests that subtle microscopic changes to a minor proportion of fiber tracts might be measured by tractography. The trend in the diffusion measures of the septo-hippocampal tracts in the lesioned compared to control animals is especially notable because the cholinergic fibers within this tract are not myelinated (Brauer et al., 2000; Gartner et al., 2001). Although axonal organization and packing may underpin the observed changes, the increase in the proportion of myelinated fibers within the

measured region may also have contributed to the trend towards an increase in mean diffusivity and axial diffusivity. Consistent with this idea, demyelination of the corpus callosum has been shown to result in decreased axial diffusivity with no change in radial diffusivity (Wu et al., 2007). In this study we used a high-order tractography model to detect differences between groups; however the small animal numbers in each group limited the power of our analysis.

Although the FA has been widely used as a measure to assess the integrity of brain connections (Kiuchi et al., 2009; Pievani et al., 2010; Teipel et al., 2010), we did not observe any trends toward significance in this parameter in our study. In these studies FA has been used to assess white matter integrity. However in our case, when measuring the septo-hippocampal tracts, the FA will mainly reflect myelinated axons rather than the unmyelinated cholinergic tracts. Hence we observed the highest trend toward significance in an increase of radial diffusivity, but no change in FA. Indeed the significant increase in radial diffusivity in the fornix in MCI and Alzheimer's disease patients compared to healthy controls found by Pievani et al. (2010) may have been caused by degeneration of the cholinergic axons. In addition, significant changes in the integrity of tracts originating in the basal forebrain have been observed in Alzheimer's disease patients using tract-based spatial statistics, where measures of tract integrity were determined based on the FA parameter (Teipel et al., 2010). However, as cholinergic fibers are not myelinated, we suggest that use of radial diffusivity measures rather than FA, using either tractography or tract-based spatial statistics analyses, may be the most sensitive parameter to discern cholinergic axonal degeneration in the fornix.

In neurodegenerative conditions such as Alzheimer's disease, axonal dystrophy and retraction occur early and may be reversible (Burek and Oppenheim, 1996). In the current study, the death of cholinergic neurons was mediated through administration of the toxin mu-p75-SAP such that axonal degeneration occurred coincidental or subsequent to cell body loss. Our findings of trends toward significant changes to diffusion parameters in the septo-hippocampal streamlines nonetheless serve as proof of principle that a moderate loss of cholinergic fibers

within the fornix can result in changes to radial diffusion parameters, and thus early changes associated with neurodegeneration may be observable even if the cell bodies are not yet lost. We therefore conclude that tractography shows promising sensitivity as a diagnostic tool for detecting pathological changes in the neuronal integrity of this fiber tract in humans, although such extrapolation remains to be further validated. Nonetheless, a recent study indicates that volumetric measurement of the basal forebrain already has diagnostic value beyond hippocampal volume measurements (Grothe et al., 2011)**.** dMRI methods may enable diagnosis of brain changes that occur as a prelude to or are a risk factor for Alzheimer's disease prior to structural changes and cognitive decline. This in turn could inform clinical treatment with acetylcholine esterase inhibitor drugs at a time at which they are likely to be most efficacious for patients.

5. Conclusions

Our study demonstrates that a ~30% loss of basal forebrain cholinergic neurons is highly correlated to the changes in water diffusion in the basal forebrain area. In addition, cholinergic neurodegeneration could be detected by analyzing diffusion parameters of the streamlines of the septo-hippocampal tracts in a mouse model. This is the first study, to our knowledge, to show the direct relationship between neuronal cell count, one of the most basic methods of measuring pathology, and diffusion MRI parameters in a disease scenario. This provides an important step forward in validating dMRI as a diagnostic imaging tool for the detection of subtle neurodegenerative events. Given that cholinergic basal forebrain degeneration is an early feature of Alzheimer’s disease, our findings demonstrate the potential feasibility of combining conventional dMRI with tractography as a non-invasive diagnostic tool to analyze both regional brain changes and variations in connectivity as a method to detect degeneration prior to detecting volumetric changes by structural MRI.

Acknowledgements

This project was funded by the Queensland State Government National and International Research Alliances Program. Adam S. Hamlin and Elizabeth J.

Coulson were supported by National Health and Medical Research Council of Australia fellowships. We thank Maree Smith, Andrew Whittaker and Ian Brereton for helpful discussions. The authors acknowledge the facilities, scientific and technical assistance of the Queensland NMR Network, and National Imaging Facility Node at the Centre for Advanced Imaging, The University of Queensland, a facility funded by the University, Queensland State and Australian Commonwealth Governments.

6. References

Berger-Sweeney, J., Stearns, N.A., Murg, S., Floerke-Nashner, L.R., Lappi, D.A., Baxter, M.G., 2001. Selective immunolesions of cholinergic neurons in mice: effects on neuranatomy, neurochemistry, and behavior. Journal of Neuroscience 21, 8164-8173.

Brauer, K., Hartig, W., Gartner, U., Bruckner, G., Arendt, T., 2000. Different myelination of rat septohippocampal fibres as revealed by immunofluorescence double-labelling. Brain Research 878, 188-193.

Burek, M.J., Oppenheim, R.W., 1996. Programmed cell death in the developing nervous system. Brain Pathology 6, 427-446.

Cole, A.E., Nicoll, R.A., 1984. Characterization of a slow cholinergic post-synaptic potential recorded in vitro from rat hippocampal pyramidal cells. Journal of Physiology 352, 173-188.

Filippi, M., Agosta, F., 2011. Structural and functional network connectivity breakdown in Alzheimer's disease studied with magnetic resonance imaging techniques. Journal of Alzheimer's Disease 24, 455-474.

Franklin, K.J.B., Paxinos, G., 2007. The Mouse Brain in Stereotaxic Coordinates Third Edition. Academic Press, San Diego.

Gartner, U., Hartig, W., Brauer, K., Bruckner, G., Arendt, T., 2001. Immunofluorescence and immunoelectron microscopic evidence for differences in myelination of GABAergic and cholinergic septohippocampal fibres. International Journal of Developmental Neuroscience 19, 347-352.

George, S., Mufson, E.J., Leurgans, S., Shah, R.C., Ferrari, C., Detoledo-Morrell, L., 2009. MRI-based volumetric measurement of the substantia innominata in amnestic MCI and mild AD. Neurobiology of Aging, doi:10.1016/j.neurobiolaging.2009.1011.1006.

Grothe, M., Heinsen, H., Teipel, S.J., 2011. Atrophy of the cholinergic basal forebrain over the adult age range and in early stages of Alzheimer's disease. Biological Psychiatry, (in press) doi:10.1016/j.biopsych.2011.1006.1019.

Grothe, M., Zaborszky, L., Atienza, M., Gil-Neciga, E., Rodriguez-Romero, R., Teipel, S.J., Amunts, K., Suarez-Gonzalez, A., Cantero, J.L., 2010. Reduction of basal forebrain cholinergic system parallels cognitive impairment in patients at high risk of developing Alzheimer's disease. Cerebral Cortex 20, 1685-1695.

Hall, A.M., Moore, R.Y., Lopez, O.L., Kuller, L., Becker, J.T., 2008. Basal forebrain atrophy is a presymptomatic marker for Alzheimer's disease. Alzheimer's & Dementia 4, 271-279.

Jones, D.K., 2010. Challenges and limitations of quantifying brain connectivity in vivo with diffusion MRI. Imaging in Medicine 2, 341-355.

Jones, D.K., Horsfield, M.A., Simmons, A., 1999. Optimal strategies for measuring diffusion in anisotropic systems by magnetic resonance imaging. Magnetic Resonance in Medicine 42, 515-525.

Kiuchi, K., Morikawa, M., Taoka, T., Nagashima, T., Yamauchi, T., Makinodan, M., Norimoto, K., Hashimoto, K., Kosaka, J., Inoue, Y., Inoue, M., Kichikawa, K., Kishimoto, T., 2009. Abnormalities of the uncinate fasciculus and posterior cingulate fasciculus in mild cognitive impairment and early Alzheimer's disease: a diffusion tensor tractography study. Brain Research 1287, 184-191.

Kokjohn, T.A., Roher, A.E., 2009. Amyloid precursor protein transgenic mouse models and Alzheimer's disease: understanding the paradigms, limitations, and contributions. Alzheimer's & Dementia 5, 340-347.

Mancuso, C., Siciliano, R., Barone, E., Butterfield, D.A., Preziosi, P., 2011. Pharmacologists and Alzheimer disease therapy: to boldly go where no scientist has gone before. Expert Opinion on Investigational Drugs 20, 1243-1261.

Melhem, E.R., Mori, S., Mukundan, G., Kraut, M.A., Pomper, M.G., van Zijl, P.C., 2002. Diffusion tensor MR imaging of the brain and white matter tractography. American Journal of Roentgenology 178, 3-16.

Mesulam, M.M., Mufson, E., Levey, A.I., Wainer, B.H., 1983. Cholinergic innervation of cortex by the basal forebrain: cytochemistry and cortical connectinos of the septal area, diagonal band nuclei, nucleus basalis (substantia innominata), and hypothalamus in the rhesus monkey. Journal of Comparative Neurology 214, 170-197.

Moldrich, R.X., Pannek, K., Hoch, R., Rubenstein, J.L., Kurniawan, N.D., Richards, L.J., 2010. Comparative mouse brain tractography of diffusion magnetic resonance imaging. NeuroImage 51, 1027-1036.

Moreau, P.H., Cosquer, B., Jeltsch, H., Cassel, J.C., Mathis, C., 2008. Neuroanatomical and behavioral effects of a novel version of the cholinergic immunotoxin mu p75-saporin in mice. Hippocampus 18, 610-622.

Mori, S., Zhang, J., 2006. Principles of diffusion tensor imaging and its applications to basic neuroscience research. Neuron 51, 527-539.

Mufson, E., 2003. Human cholinergic basal forebrain: chemoanatomy and neurologic dysfunction. Journal of Chemical Neuroanatomy 26, 233-242.

Mufson, E., Bothwell, M., Hersh, L.B., Kordower, J.H., 1989. Nerve growth factor receptor immunoreactive profiles in the normal, aged human basal forebrain: colocalization with cholinergic neurons. The Journal of Comparative Neurology, 196-217.

Mufson, E.J., Ma, S.Y., Dills, J., Cochran, E.J., Leurgans, S., Wuu, J., Bennett, D.A., Jaffar, S., Gilmor, M.L., Levey, A.I., Kordower, J.H., 2002. Loss of basal forebrain $P75^{NTR}$ immunoreactivity in subjects with mild cognitive impairment and Alzheimer's disease. Journal of Comparative Neurology 443, 136-153.

Muth, K., Schonmeyer, R., Matura, S., Haenschel, C., Schroder, J., Pantel, J., 2010. Mild cognitive impairment in the elderly is associated with volume loss of the cholinergic basal forebrain region. Biological Psychiatry 67, 588-591.

Nilsson, O.G., Leanza, G., Rosenblad, C., Lappi, D.A., Wiley, R.G., Bjorklund, A., 1992. Spatial learning impairments in rats with selective immunolesion of the forebrain cholinergic system. Neuroreport 3, 1005-1008.

Perry, T.A., Hodges, H., Gray, J.A., 2001. Behavioural, histological and immunocytochemical consequences following 192 IgG-saporin immunolesions of the basal forebrain cholinergic system. Brain Research Bulletin 54, 29-49.

Pierpaoli, C., Jezzard, P., Basser, P.J., Barnett, A., Di Chiro, G., 1996. Diffusion tensor MR imaging of the human brain. Radiology 201, 637-648.

Pievani, M., Agosta, F., Pagani, E., Canu, E., Sala, S., Absinta, M., Geroldi, C., Ganzola, R., Frisoni, G.B., Filippi, M., 2010. Assessment of white matter tract damage in mild cognitive impairment and Alzheimer's disease. Human Brain Mapping 31, 1862-1875.

Rossner, S., 1997. Cholinergic immunolesions by 192-IgG-Saporin - A useful tool to stimulate pathogenic aspects of Alzheimer's disease. International Journal of Developmental Neuroscience 15, 835-850.

Sara, S.J., 2009. The locus coeruleus and noradrenergic modulation of cognition. Nature Reviews Neuroscience 10, 211-223.

Teipel, S.J., Meindl, T., Grinberg, L., Grothe, M., Cantero, J.L., Reiser, M.F., Moller, H.J., Heinsen, H., Hampel, H., 2010. The cholinergic system in mild cognitive impairment and Alzheimer's disease: An in vivo MRI and DTI study. Human Brain Mapping 32, 1349-1362.

Tuch, D.S., Salat, D.H., Wisco, J.J., Zaleta, A.K., Hevelone, N.D., Rosas, H.D., 2005. Choice reaction time performance correlates with diffusion anisotropy in white matter pathways supporting visuospatial attention. Proceedings of the National Academy of Sciences of the United States of America 102, 12212-12217.

Wainer, B.H., Levey, A.I., Rye, D.B., Mesulam, M.M., Mufson, E.J., 1985. Cholinergic and non-cholinergic septohippocampal pathways. Neuroscience Letters 54, 45-52.

Whitehouse, P.J., Price, D.L., Struble, R.G., Clark, A.W., Coyle, J.T., Delon, M.R., 1982. Alzheimer's disease and senile dementia: loss of neurons in the basal forebrain. Science 215, 1237-1239.

Wu, Q., Butzkueven, H., Gresle, M., Kirchhoff, F., Friedhuber, A., Yang, Q., Wang, H., Fang, K., Lei, H., Egan, G.F., Kilpatrick, T.J., 2007. MR diffusion changes correlate with ultra-structurally defined axonal degeneration in murine optic nerve. NeuroImage 37, 1138-1147.

Ypsilanti, A.R., Girao da Cruz, M.T., Burgess, A., Aubert, I., 2008. The length of hippocampal cholinergic fibers is reduced in the aging brain. Neurobiology of Aging 29, 1666-1679.

Figure captions

Table 1. Septo-hippocampal connections remained unchanged for track volume, streamline length and normalized streamline number in lesioned animals. n = 4 per group, mean ± SEM

Table 2. The toxin showed no effect on track volume, streamline length and normalized streamline number of the inferior cerebellar peduncle for lesioned animals compared to control animals. n = 4 per group, mean ± SEM

Figure 1. Intracerebroventricular application of mu-p75-saporin produced a specific lesion of basal forebrain cholinergic neurons. **A**. Mean (± SEM) total number of ChAT-positive neurons in the basal forebrain following application of mu-p75-SAP (Lesion, n = 4) or Rb-IgG-SAP (Control, n = 4). A significant decrease in the number of ChAT-positive neurons was found following application of mu-p75-SAP. **B**. Mean (± SEM) number of parvalbumin-positive neurons in the basal forebrain following application of mu-p75-SAP (n = 4) or Rb-IgG-SAP (n = 3). Application of mu-p75-SAP had no effect on the number of parvalbumin-positive neurons. **C.** Photomicrographs of ChAT-immunopositive neuronal cell bodies in the basal forebrain and ChAT-immunoreactive terminal fields in the hippocampus following application of Rb-IgG-SAP (left) and mu-p75-SAP (right). **D**. Photomicrographs of parvalbumin-immunopositive neuronal cell bodies in the medial septum and vertical diagonal band of Broca following application of Rb-IgG-SAP (left) and mu-p75-SAP (right). Scale bar = 400µm. * $p<0.05$

Figure 2. Basal forebrain mask encompassing the medial septum, and the vertical and horizontal diagonal bands of Broca. The position of the basal forebrain mask (red) in MRI space is shown in three planes: **A.** sagittal (midline),

B. horizontal (level of anterior commissure crossing the midline), and **C-E.** coronal sections through the extent of the basal forebrain depicting the mask at approximately 1.10 mm **(C)**, 0.86 mm **(D)** and 0.50 mm **(E)** anterior to Bregma. The mask was used as a volume to extract diffusion parameters for the basal forebrain and as a seed region for tractography streamlines.

Figure 3. The mean FA, mean diffusivity, axial diffusivity and radial diffusivity values of lesioned animals in the area of the basal forebrain mask inversely correlated to the cholinergic neuron number in the basal forebrain. A comparison of group means of diffusion parameters for lesioned and control animals revealed that **A**. FA (mean ± SEM), **B.** mean diffusivity (mean ± SEM), **C.** axial diffusivity (mean ± SEM) and **D.** radial diffusivity (mean ± SEM) values were significantly increased for the basal forebrain of lesioned compared to control animals. Linear regression analysis of ChAT-positive neuron number (x-axis) to the previously mentioned diffusion parameters (y-axis) of individual animals of mu-p75-SAP (lesion) and Rb-IgG-SAP (control) groups revealed a significant inverse correlation of **E.** FA, **F.** mean diffusivity, **G.** axial diffusivity, as well as **H.** radial diffusivity parameters with ChAT-positive neuron number. n = 4 per group, * $p<0.05$; unit for mean diffusivity, axial diffusivity and radial diffusivity is [10^{-4} mm^2/s].

Figure 4. Tractography streamlines connecting the basal forebrain and hippocampus. The basal forebrain mask shown in Figure 3 was used as a seed region to generate a streamline profile of the basal forebrain and further delineated to only measure septo-hippocampal connections (yellow), shown in sagittal **(A)**, coronal **(B)** and horizontal **(C)** planes. To achieve this, a hippocampus waypoint ROI at the level of **(a)** as indicated by the dashed line, was applied. **D.** A slice through the streamline profile is shown to validate the regions of the highest fiber density. Most streamlines were found to pass through the alveus (alv) and the oriens layer of the hippocampus (or) which are known to

contain fimbria/fornix output from pyramidal neurons and the septal/diagonal band input to basal dendrites of pyramidal neurons, respectively. A very small proportion of streamlines were found to project to areas such as the cingulum, CA1-3 and other regions of the hippocampus. Additional abbreviations: cg, cingulum; cp, cerebellar peduncle; DG, dentate gyrus; fmj, forceps major of the corpus callosum; MoDG, molecular layer of the dentate gyrus.

Figure 5. Increased MD and RD of septo-hippocampal streamlines after lesion of the cholinergic basal forebrain. Diffusion parameters for the streamlines shown in Figure 4 were analyzed, revealing that FA **(A)** and axial diffusivity **(B)** parameters were not significantly different between control and lesioned animals, whereas radial diffusivity **(C)** and mean diffusivity **(D)** values showed trends toward a significant increase in the lesioned animals. n = 4 per group; unit for mean diffusivity, axial diffusivity and radial diffusivity is [10^{-4} mm^2/s].

Figure 6. Tractography of the inferior cerebellar peduncle, a white matter tract that should not be affected by the toxin-induced lesion or the surgery itself, shown in MRI space in coronal **(A)** and horizontal **(B)** planes. No changes in control vs. lesioned animals were observed for FA **(C)**, axial diffusivity **(D)**, radial diffusivity **(E)** or mean diffusivity **(F)**. n = 4 per group; unit for mean diffusivity, axial diffusivity and radial diffusivity is [10^{-4} mm^2/s].

Table 1

Parameter	Control	Lesion	Significance (p value)
Track volume (voxels)	11055 ± 459	11115 ± 396	0.89
Streamline length (mm)	10.25 ± 0.09	10.12 ± 0.02	0.34
Normalized streamline number	1.30 ± 0.06	1.27 ± 0.08	0.69

Table 2

Parameter	Control	Lesion	Significance (p value)
Track volume (voxels)	21682 ± 430	19876 ± 1290	0.86
Streamline length (mm)	10.15 ± 0.23	10.12 ± 0.28	0.34
Normalized streamline number	117.25 ± 7.30	123.07 ± 7.30	0.69

Figure 1

Click here to download 9. Figure: Kerbler-Figure_1.pdf

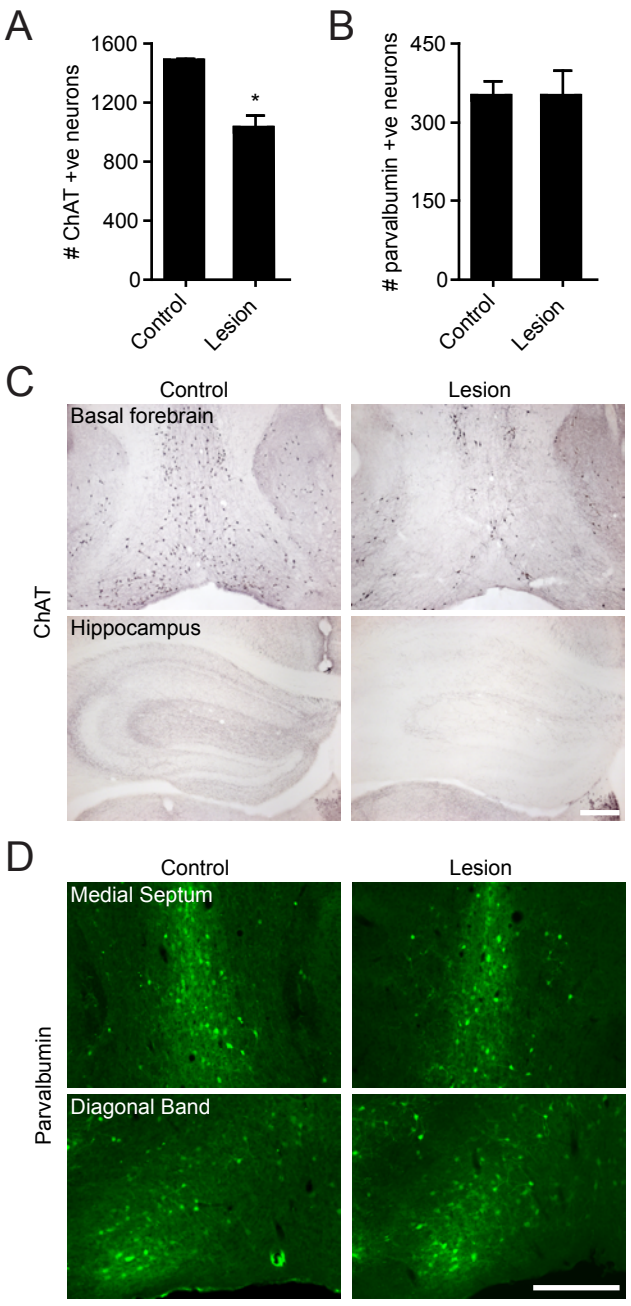

Figure 2

Click here to download 9. Figure: Kerbler-Figure_2.pdf

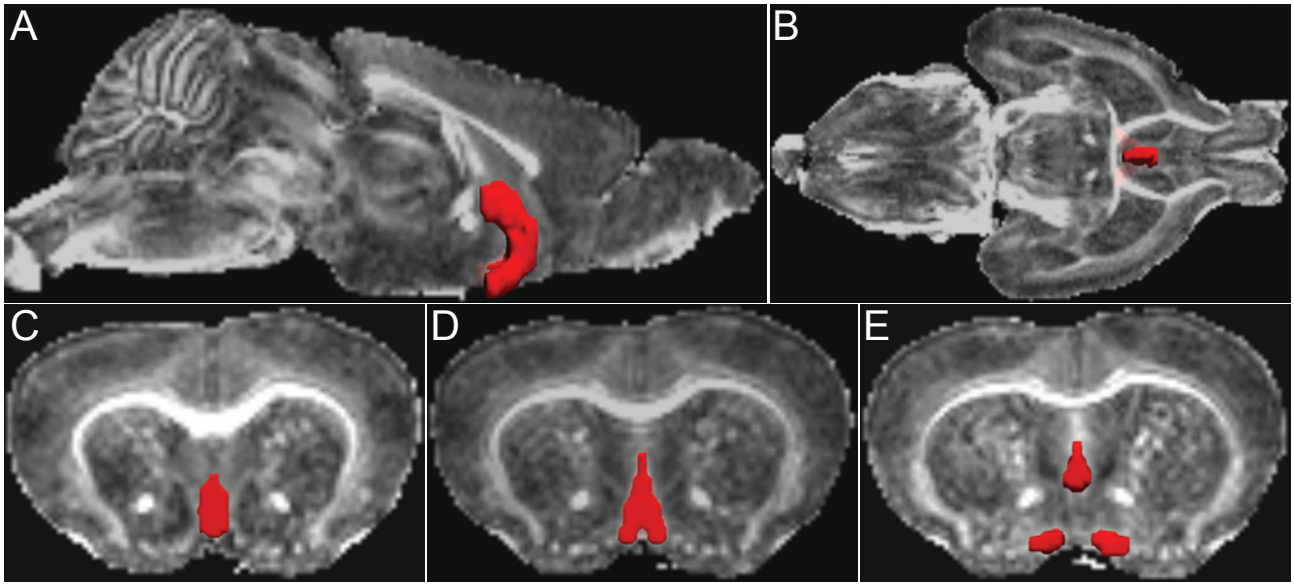

Figure 3

Click here to download 9. Figure: Kerbler-Figure_3.pdf

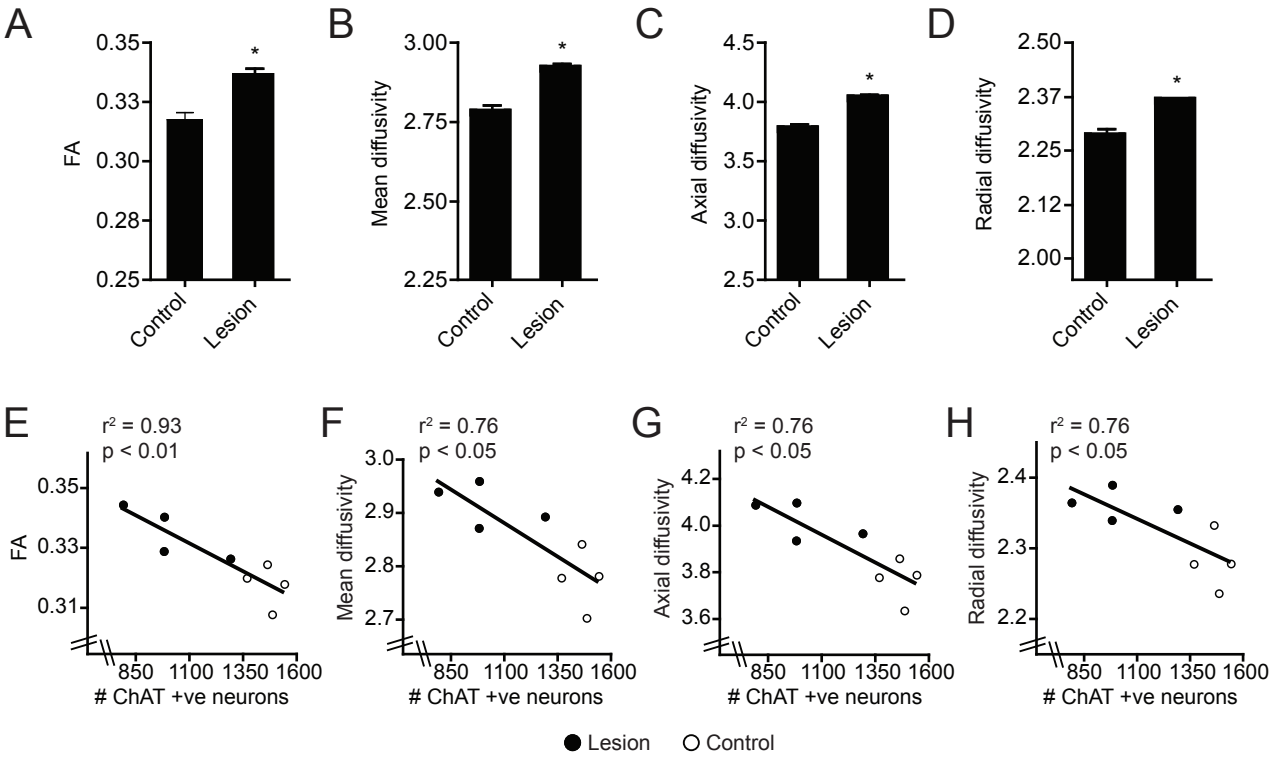

Figure 4

Click here to download 9. Figure: Kerbler-Figure_4.pdf

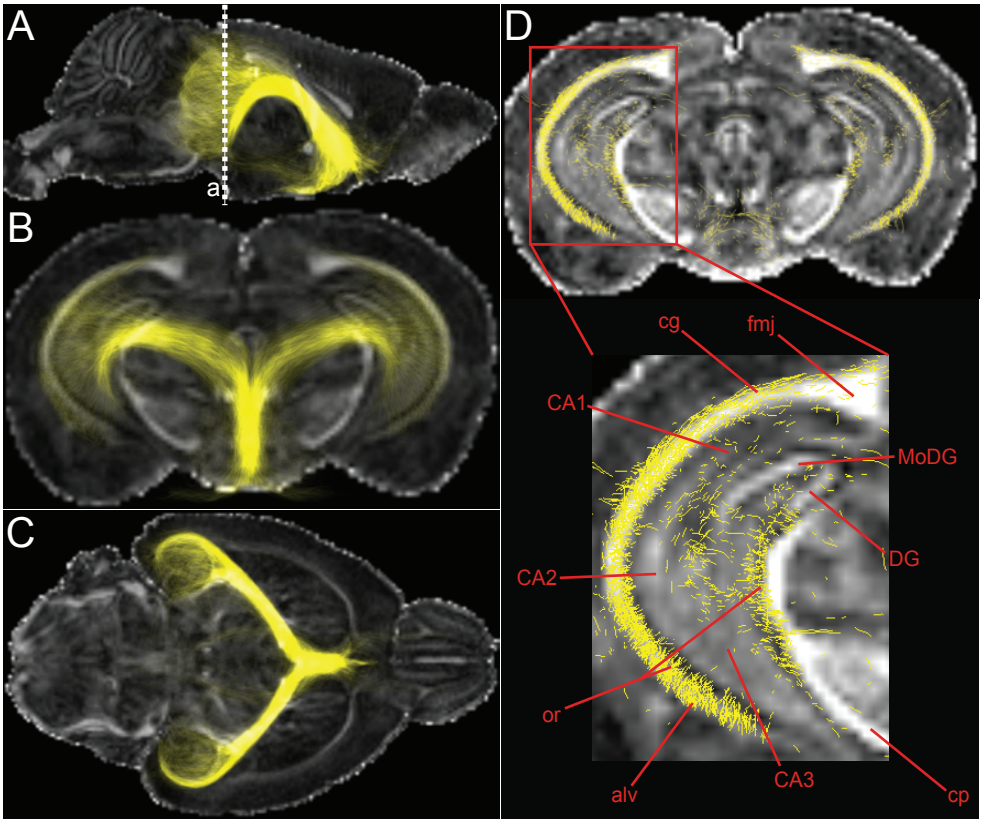

Figure 5

Click here to download 9. Figure: Kerbler-Figure_5.pdf

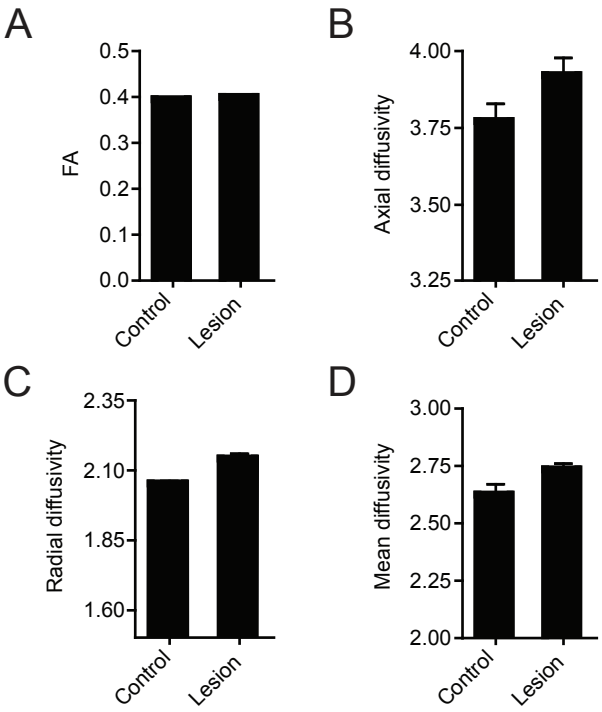

Figure 6

Click here to download 9. Figure: Kerbler-Figure_6.pdf